

# EMHD flow of second-grade fluid through a heated permeable disk with space dependent heat source

Proc IMechE Part E:

J Process Mechanical Engineering

1–12

© IMechE 2023

Article reuse guidelines:

sagepub.com/journals-permissions

DOI: 10.1177/09544089231159203

journals.sagepub.com/home/pie



Kohta Gangadhar<sup>1</sup> , M. Rupa Lavanya<sup>1</sup>  and Ali J. Chamkha<sup>2</sup>

## Abstract

In this article, von Kármán MHD viscoelastic fluid flow with second-grade model through a heated permeable disk on electric field is examined thoroughly. The effects of viscous dissipation and elasticity on fluid motion around the disk, temperature and space-dependent heat source/sink are also examined. Governing partial differential equations are transmitted into ordinary differential equations with similarity functions. Later, nonlinear system of ordinary differential equations was solved with the help of Galerkin finite element method. Accuracy and validity of the method were noticed by comparing our results with the previous literature. Simulations are performed in order to capture the dynamics of the physical situations against the variation of the pertinent parameters. Nature of heat flux and stresses of the physical parameters are discussed. Physical influence of heat flux, heat transfer is exhibited graphically at the surface of disk and increases when the values of Prandtl number are increased, whereas there is a decreasing trend in the rate of heat transfer when the value of Eckert number is increased.

## Keywords

von Kármán flow, variable surface temperature, GFEM, viscoelastic fluid, electric field

Date received: 16 June 2022; accepted: 6 February 2023

## Introduction

The stability of magnetic and electric fields supplied for inconceivable influence of implementation in sciences, engineering, and medicine. Disparate industrial devices from pumps, bearings, MHD generators along with the boundary layer control impact on communication among the electrical conduction fluid and the magnetic field. Daniel et al.<sup>1</sup> inspected the role of electric field and the impact of error mechanism about the unstable flow of electrical nanofluid over a stretched sheet. They found to velocity had a blunt adverse communication of electric and magnetic fields. Mardani et al.<sup>2</sup> investigated numerically the droplet coalescence of salt water in crude oil by extraneous magnetic field. Sun et al.<sup>3</sup> established the heat transfer model by electrochromatography into transverse electric field. Khazayinejad and Nourazar<sup>4</sup> presented dimensional constituent heat transfer for MHD boundary layer flow of hybrid nanofluid with Fourier's law of heat direction working optimal collocation method. Urgorri et al.<sup>5</sup> analyzed the MHD boundary layers of tritium concentration to PbLi flows. They examined mass transport through MHD boundary layers is increased by the magnetic field up to an asymptotic value. Zhang et al.<sup>6</sup> considered the consequence of second-harmonic propagation covered by external magnetic field and electric field about parabolic quantum dots. Yan et al.<sup>7</sup> discussed the efficiency spectrum

of busmethene quantum dots to the existence of in-plane electric and transfer fields by the tight-binding method. Zakaria et al.<sup>8</sup> scrutinized the instability analysis by the viscous liquid sheet covered by the consequence of a tangential electric field. The irreversibility analysis by MHD boundary layer flow of Maxwell nanofluid past the reducing surface was studied by Siddiqui et al.<sup>9</sup> The two-dimensional aligned MHD incompressible movement of nanoliquids close to absorptive stretched sheet that the existence of Joule heating was scrutinized by Riaz Khan et al.<sup>10</sup> Korei et al.<sup>11</sup> inspected by MHD mixed convection boundary layer flow of hybrid nanofluids in a moderately heated lid-driven cavity.

In previous literature, researchers used non-Newtonian fluid mechanics to data the differing components and presences of such fluids. Even subsequent Navier–Stokes equations are the complications are recorded as

<sup>1</sup>Department of Mathematics, AcharyaNagarjuna University Campus, Ongole, Andhra Pradesh, India

<sup>2</sup>Faculty of Engineering, Kuwait College of Science and Technology, Doha, Kuwait

### Corresponding author:

Ali J. Chamkha, Faculty of Engineering, Kuwait College of Science and Technology, Doha District 35004, Kuwait.

Email: a.chamkha@kcst.edu.kw

the existence of nonlinear restricted terms. Although viscosity was variable entrenched in enforced effort or stress, it might be restricted by non-Newtonian fluid. The frequent every day examples are maize starch deteriorated in water. Newtonian fluid behaviors similarly water could be supposed entirely as pressure or temperature. However, the non-Newtonian fluids physical behavior calculates in the force this conduct on it from time to time. A number of non-Newtonian fluids had generated the confusing rheology of common liquids. Non-Newtonian fluids had newly seized tremendous importance in industrial, mechanical and commercial applications. These liquids are worked in material handling, food processing, oil storage, chemical processes, and many others. Products such as ketchup, blood, oils, and mud than and dense liquids are restricted by non-Newtonian fluids. A subdivision of non-Newtonian liquids combines liquids holding memory effects that are labeled by viscoelastic fluids. In similar fluids, fluid motion is not only averred as the current stress state but also by the strain history of volume element. The second-grade model had last generally studied to evaluate viscoelastic effects in numerous boundary layer problems. Burhan Jafeer and Mustafa<sup>12</sup> considered the von-Karman flow of viscoelastic fluid by the heated permeable disk. The problem of magnetized flow about an Oldroyd-B fluid by a rotating disk had considered as Hafeez et al.<sup>13</sup> A mixed convection of viscoelastic fluids in a lid-driven cavity was investigated by Gupta et al.<sup>14</sup> Hernandez<sup>15</sup> studied the thermo-diffusive effect on electro osmotic flow of a viscoelastic fluid in the slash microchannel. Even torque and thrust of propellers in viscoelastic fluids were studied by Cao et al.<sup>16</sup> Finally, numerous researchers had do their work in viscoelastic fluid as taking distant physical effects those are displayed by Refs.<sup>17–25</sup>

Heat transfer of magneto hydrodynamic flow is extremely concerned with the heat dissipation phenomenon (heated dissipated being friction forces) and Ohmic dissipation (heat dissipated as Joule heating). Numerous modules had been assisted and applicable to the literature. In case, Nazir et al.<sup>26</sup> discussed the time-dependent Casson fluid flow exposure for magnetic field and variable time and space-dependent temperature. Singh et al.<sup>27</sup> explored the consequences of nonuniform surface heating to the common delegation that the Casson fluid past the vertical cone with viscous dissipation. Mburu et al.<sup>28</sup> performed an entropy analysis for three-dimensional MHD Oldroyd-B fluid flow for the effects of a mixed chemical reaction and viscous dissipation. Gangadhar et al.<sup>29</sup> explored the stagnation point slip flow of a hybrid nanofluid with convective condition and viscous dissipation. The problem of boundary layer flow of nanofluid over an exponentially stretched surface with variable suction was scrutinized by Rao et al.<sup>30</sup> Even destruction minimization in MHD flow of a Williamson nanofluid flow past the flexible surface with viscous heating is considered as Gangadhar et al.<sup>31</sup> Hamid et al.<sup>32</sup> discussed the ferrofluid transport previous the enterable nonisothermal emotional surface to the

viscous dissipation effect. Ajibade and Umar<sup>33</sup> presented the influence of wall condition and viscous dissipation to calculate common delegation Couette flow in a vertical channel to a few density to the detention slabs. Under the influence of Joule heating and viscous dissipation for embellished thermal efficiency for copper–aluminum oxide nanoparticles was considered as Abbasi et al.<sup>34</sup> Salawu et al.<sup>35</sup> calculated the viscous dissipation effect on magneto-Oldroyd-8 constant material with a double exothermic reaction.

Mathematical illustration in a rotating disk complication was essential over the wide range in science, engineering, and product design appositeness. MHD flow near a rotating disk is presented as Ariel.<sup>36</sup> Even magneto-hydrodynamic rotating disk flow by the non-Newtonian Reiner–Rivlin authority of fluid with ion slip effect has been conducted by Attia.<sup>37</sup> Guha and Sengupta<sup>38</sup> studied the von Karman flow of the rotating disk from Bingham fluids. Kumar et al.<sup>39</sup> discussed for swirling flow about the nanoliquid through the radially flexible rotating disk among the deliberation of Arrhenius chemical reaction. The existence of diffusivity of gases and liquids nearby rotating disk for temperature-dependent viscosity was performed by Khan et al.<sup>40</sup> Mabood et al.<sup>41</sup> considered Stefan blowing influence on incompressible hydromagnetic flow of Maxwell nanofluid by variable thermal conductivity.

By the motivation of previous researchers, we had depicted the hydrothermal variations of second-grade fluid above a revolving disk in the electric field. Joule heating and viscous dissipation are combined to analyze the hydrothermal principle at the flow. As well as, even variable surface temperature acceptance was just popularized in that paper. Later complete literature, the physical position was averred and modeled. Establishing exotic flow fields (temperature and velocity) is determined through corrective shaped nonlinear mathematical problems for finite element method (FEM). Finite element method was a capable technique for had been strongly furnished to CFD problems.<sup>26,42</sup> Since numerical simulation code was approved and documented to study with earlier broadcasted benchmark. The abundance of engineering activity namely increasing Nusselt number and wall share is examined by differing choices of regulating parameters. The perfect examination is shortly averred at the end of this article.

## Problem formulation

Considered a steady laminar electrical MHD viscoelastic fluid flow rotating around the large disk of radius  $R$  with the consistent angular speed  $\omega$ . Let  $(u_1, v_1, w_1)$  remain the extension of velocity vector as azimuthal, radial, and axial axes, appropriately, to cylindrical coordinate system  $(r_1, \varphi_1, z_1)$ . Fluid flow was proposed when the homogeneous rotation about the almost large disk around axial coordinate  $z_1$ . Now modesty, we expect that disk was regular to the plane  $z_1 = 0$  during fluid was supplied to semi-infinite region  $z_1 \geq 0$  (look at

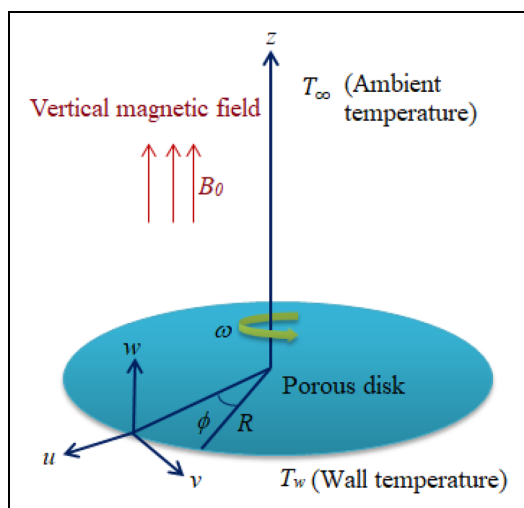


Figure 1. Physical figure about the problem.

Figure 1). Axial symmetry of the complication permits one to avoid innovation of velocity that azimuthal directions. In homogenous magnetic field if flux density  $B_0$  and electric field of flux density  $E_0$  are applied perpendicular through every flow order. The convinced magnetic field included by the assumptions about the small magnetic Reynolds number.

Under a boundary layer approximations could be costly in the consecutive terms (look at Ariel et al.<sup>36</sup> being derivation about stress tensor components):

$$\frac{\partial u_1}{\partial r_1} + \frac{u_1}{r_1} + \frac{\partial w_1}{\partial z_1} = 0, \quad (1)$$

$$u_1 \frac{\partial u_1}{\partial r_1} + w_1 \frac{\partial u_1}{\partial z_1} - \frac{v_1^2}{r_1^2} = \nu \frac{\partial^2 u_1}{\partial z_1^2} + \frac{\alpha_1}{\rho_0} \left[ u_1 \frac{\partial^3 u_1}{\partial r_1 \partial z_1^2} + w_1 \frac{\partial^3 u_1}{\partial z_1^3} + \frac{\partial u_1}{\partial r_1} \frac{\partial^2 u_1}{\partial z_1^2} \right] + \frac{\alpha_1}{\rho_0} \left[ -\frac{\partial u_1}{\partial z_1} \frac{\partial^2 w_1}{\partial z_1^2} + \frac{\partial^2 v_1}{\partial z_1^2} \left( \frac{\partial v_1}{\partial r_1} - \frac{v_1}{r_1} \right) \right] + \frac{\sigma}{\rho_0} (E_0 B_0 - B_0^2 u_1), \quad (2)$$

$$u_1 \frac{\partial v_1}{\partial r_1} + w_1 \frac{\partial v_1}{\partial z_1} + \frac{u_1 v_1}{r_1} = \nu \frac{\partial^2 v_1}{\partial z_1^2} + \frac{\alpha_1}{\rho_0} \left[ -\frac{\partial v_1}{\partial z_1} \frac{\partial^2 u_1}{\partial r_1 \partial z_1} + u_1 \frac{\partial^3 v_1}{\partial r_1 \partial z_1^2} + w_1 \frac{\partial^3 v_1}{\partial z_1^3} \right] + \frac{\alpha_1}{\rho_0} \left[ \frac{u_1}{r_1} \frac{\partial^2 v_1}{\partial z_1^2} - \frac{\partial v_1}{\partial z_1} \frac{\partial^2 w_1}{\partial z_1^2} - \frac{1}{r_1} \frac{\partial u_1}{\partial z_1} \frac{\partial v_1}{\partial z_1} \right] + \frac{\sigma}{\rho_0} (E_0 B_0 - B_0^2 v_1), \quad (3)$$

Here,  $\sigma$  displays fluid electrical conductivity,  $\rho_0$  is labeled just as density,  $\nu$  grandstands as coefficient of kinematic viscosity, and  $\alpha_1 > 0$  remain a material constant that arrears about viscoelasticity based on the fluid.

Therefore, every surface does absorptive and performance no error, from Burhan Jafeer and Mustafa<sup>12</sup>:

$$z_1 = 0: u_1 = 0, v_1 = r_1 \omega, w_1 = -w_0, \quad (4)$$

The oblique velocities evaporate above the disk, one could explicit

$$z_1 \rightarrow \infty: u_1 \rightarrow 0, v_1 \rightarrow 0. \quad (5)$$

We explicit the velocities ( $u_1, v_1, w_1$ ) as:

$$u_1 = r_1 \omega F_1'(\eta), v_1 = r_1 \omega G_1(\eta), w_1 = -2\sqrt{\omega \nu} F_1(\eta), \quad (6)$$

where  $\eta = z_1 \sqrt{\omega / \nu}$  do every dimensionless essential distance, although the details  $\sqrt{\omega / \nu}$  and  $\sqrt{\omega \nu}$  are unique velocity and length scales about a problem.

Representation of certain variables popularized current Equation (6) satisfy Equation (1) although Equations (2) and (3) modification toward the following ODEs:

$$F_1''' + G_1^2 + 2F_1 F_1'' - F_1'^2 + K(2F_1' F_1''' + F_1''^2 + G_1^2 - 2F_1 F_1'''' ) + M(E_1 - F_1') = 0, \quad (7)$$

$$G_1'' - 2F_1' G_1 + 2F_1 G_1' + K(-2F_1 G_1''' + 2F_1' G_1'') + M(E_1 - G_1) = 0, \quad (8)$$

And every boundary conditions remain converted:

$$F_1(0) = S, F_1'(0) = 0, G_1(0) = 1, \quad (9)$$

$$F_1' \rightarrow 0, F_1'' \rightarrow 0, G_1 \rightarrow 0 \text{ as } \eta \rightarrow \infty, \quad (10)$$

Here,  $S = w_0 / 2\sqrt{\omega \nu}$  do the surface consumption parameter,  $K = \alpha_1 \omega / \mu$  was labeled viscoelastic fluid parameter,  $M = \sigma B_0^2 / \rho_0 \omega$  denotes the magnetic interaction parameter, and  $E_1 = E_0 / B_0 \omega$  is the electric field parameter.

Every parameter  $S$  regulates the magnitude by consumption velocity prescribed on the exterior. They could then consider values by the range of  $0 \leq S < \infty$ . The case  $S < 0$  describes the dose aspect. The parameter  $M$  measures the energy about Lorentz force and it could take several value mod the range of  $M \geq 0$ . Furthermore, parameter  $E_1$  represents the energy on electric field and it could chose several value with the range  $E_1 \geq 0$ .

### Heat transfer analysis

Burhan Jafeer and Mustafa,<sup>12</sup> heating development about the disk is described through the equilateral temperature distribution  $T_w = T_\infty + b r_1^2$  here  $b$  do the stable for dimension  $\{\Theta L^{-2}\}$  and  $T_\infty$  indicate ambient fluid

temperature. According to the viscous dissipation, heat generation, and Joule heating effects, the energy equation is disposed as:

$$\rho_0 C_p \left( u_1 \frac{\partial T}{\partial r_1} + w_1 \frac{\partial T}{\partial z_1} \right) = \kappa \frac{\partial^2 T}{\partial z_1^2} + \sigma((u_1 B_0 - E_0)^2 + (v_1 B_0 - E_0)^2) + \Phi + q''' \quad (11)$$

Boundary conditions

$$T = T_w \text{ at } z_1 = 0 \text{ and } T \rightarrow T_\infty \text{ as } z_1 \rightarrow \infty, \quad (12)$$

Here,  $\kappa$  perform a thermal conductivity,  $C_p$  signify heat capacity based on fluid by  $\Phi$  is the viscous dissipation phrase, constant pressure, and  $q'''$  is the variable heat source or sink which are defined as:

$$\begin{aligned} \Phi = & \tau_{r_1 r_1} \left( \frac{\partial u_1}{\partial r_1} \right) + \tau_{\phi_1 \phi_1} \left( \frac{u_1}{r_1} \right) + \tau_{z_1 z_1} \left( \frac{\partial w_1}{\partial z_1} \right) \\ & + \tau_{r_1 \phi_1} \left( \frac{\partial v_1}{\partial r_1} - \frac{v_1}{r_1} \right) + \tau_{\phi_1 z_1} \left( \frac{\partial v_1}{\partial z_1} \right) \\ & + \tau_{r_1 z_1} \left( \frac{\partial u_1}{\partial z_1} + \frac{\partial w_1}{\partial r_1} \right), \end{aligned} \quad (13)$$

Stress tensor appeases the second-grade exemplary.

The fourth term in the right-hand side of Equation (11), heat source or sink, and it is given by

$$q''' = \frac{\kappa u_w}{r_1 v} [A(T_w - T_\infty)F'_1 + B(T - T_\infty)], \quad (14)$$

Equation (11) along with boundary layer approximations is:

$$\begin{aligned} u_1 \frac{\partial T}{\partial r_1} + w_1 \frac{\partial T}{\partial z_1} = & \frac{\kappa}{\rho_0 C_p} \frac{\partial^2 T}{\partial z_1^2} + \frac{\mu}{\rho_0 C_p} \left\{ \left( \frac{\partial u_1}{\partial z_1} \right)^2 + \left( \frac{\partial v_1}{\partial z_1} \right)^2 \right\} + \frac{\sigma}{\rho_0 C_p} ((u_1 B_0 - E_0)^2 + (v_1 B_0 - E_0)^2) \\ & + \frac{\alpha_1}{\rho_0 C_p} \left\{ u_1 \frac{\partial u_1}{\partial z_1} \frac{\partial^2 u_1}{\partial r_1 \partial z_1} + w_1 \frac{\partial u_1}{\partial z_1} \frac{\partial^2 u_1}{\partial z_1^2} + u_1 \frac{\partial v_1}{\partial z_1} \frac{\partial^2 v_1}{\partial r_1 \partial z_1} + w_1 \frac{\partial v_1}{\partial z_1} \frac{\partial^2 v_1}{\partial z_1^2} \right\} \\ & + \frac{\kappa u_w}{r_1 v} [A(T_w - T_\infty)F'_1 + B(T - T_\infty)], \end{aligned} \quad (15)$$

Defining the nondimensional temperature as  $\theta_1(\eta) = (T - T_\infty) / (T_w - T_\infty)$ , Equation (14) takes the form

$$\begin{aligned} \frac{1}{Pr} \theta''_1 - 2F'_1 \theta_1 + 2F_1 \theta'_1 + Ec \{ (F''_1 + G_1^2) + M[(F'_1 - E_1)^2 + (G_1 - E_1)^2] \} \\ + KEc \{ F'_1 (F''_1 + G_1^2) - 2F_1 (F'_1 F''_1 + G'_1 G''_1) \} \\ + \frac{1}{Pr} (AF'_1 + B\theta_1) = 0, \end{aligned} \quad (16)$$

And the boundary conditions are changed as:

$$\theta_1(0) = 1 \text{ and } \theta_1 \rightarrow 0 \text{ as } \eta \rightarrow \infty, \quad (17)$$

where  $Pr = \mu C_p / \kappa$  represents every Prandtl number and  $Ec = \omega^2 / C_p b$  grants the Eckert number. Indication such individual present elect about rectangular surface temperature output the constant Eckert number by correspondingly self-related equation (15). Consequently note this only the narrowly identical result longing available to prevent by constant wall temperature.

Arrangement of (8)–(10), (16) and (17) collapses toward a Newtonian fluid case at  $K = 0$  since the case  $Ec = 0$  compare via a solution the heat dissipation effects remain vanished and  $A = 0 = B$  represents through every direction the heat generation effects remain vanished. Moreover, every case based on hydrodynamic flow, nonelectric field and impassable exterior obtain found at  $M = 0$ ,  $E_1 = 0$  and  $S = 0$ , subsequently. Every explanation by  $Pr$  and  $Ec$  definitely recommend this the particular could take exclusive confident values.

### Physical quantities

Flow capacity and the significance of resisting torque, drag coefficient, volumetric flow rate and wall heat transfer rate. Therefore, the above is the maximum essential appliance against engineering way of thinking. The skin friction coefficient in the radial direction was detailed come from:

$$C_{fr} = \frac{\tau_{z_1 r_1} |_{z_1=0}}{\rho_0 r_1^2 \omega^2}, \quad (18)$$

where radial stress  $\tau_{z_1 r_1}$  is given by:

$$\begin{aligned} \tau_{z_1 r_1} = & \mu \frac{\partial u_1}{\partial z_1} \\ & + \alpha_1 \left\{ u_1 \frac{\partial^2 u_1}{\partial r_1 \partial z_1} + w_1 \frac{\partial^2 u_1}{\partial z_1^2} + \frac{\partial u_1}{\partial r_1} \frac{\partial u_1}{\partial z_1} - \frac{\partial u_1}{\partial z_1} \frac{\partial w_1}{\partial z_1} + \frac{\partial v_1}{\partial z_1} \left( \frac{\partial v_1}{\partial r_1} - \frac{v_1}{r_1} \right) \right\}. \end{aligned} \quad (19)$$

Over the effecting need of Equation (6), we show up as

$$\sqrt{Re} C_{fr} = F''_1(0) - 2KF_1(0)F''_1(0), \quad (20)$$

Here,  $Re = r_1^2 \omega / \nu$  represent as local Reynolds number.

After illustrious quantities were moment coefficient detailed as displace (look at Attia<sup>37</sup>):

$$C_{m,r} = \frac{T_r}{\rho_0 \omega^2 r_1^5}, \quad (21)$$

Here, the torque necessary  $T_r$  is calculated as result:

$$T_r = \int_0^{r_1} \tau_{z_1 \theta_1} |_{z_1=0} 2\pi r_1^2 dr_1, \quad (22)$$

In which  $\tau_{z_1 \theta_1}$  is azimuthal stress which is obtained as:

$$\tau_{z_1 \theta_1} = \mu \frac{\partial v_1}{\partial z_1} + \alpha_1 \left\{ u_1 \frac{\partial^2 v_1}{\partial r_1 \partial z_1} + w_1 \frac{\partial^2 v_1}{\partial z_1^2} + \frac{u_1}{r_1} \frac{\partial v_1}{\partial z_1} - \frac{\partial v_1}{\partial z_1} \frac{\partial w_1}{\partial z_1} \right\}. \quad (23)$$

Conjure revolution (6), we appear by the subsequent

$$\sqrt{\text{Re}} C_{m,r} = \frac{\pi}{2} (G'_1(0) - 2K F_1(0) G''_1(0)), \quad (24)$$

Significant every Nusselt number is

$Nu = -LK \left( \frac{\partial T}{\partial z_1} \right)_{z_1=0} / (T_w - T_\infty)^{38}$  with  $L = \sqrt{v/\omega}$  is the unique length scale, they collect the ensuing

$$Nu = -\theta'_1(0). \quad (25)$$

Therefore, the disk drag fluid of the vertical direction by the rate of  $\omega(\infty)$ , pumping efficiency on finite disk among radius  $R$  could be determined against the obvious essential:

$$Q = \int_0^R -\omega(\infty) 2\pi r_1 dr_1 = 2\sqrt{v\omega} F(\infty) \pi R^2. \quad (26)$$

The set of Equations (20)–(26) definitely recommend a certain single had toward intently inspect the variation by  $F'_1(0)$ ,  $G'_1(0)$ ,  $\theta'_1(0)$  and  $F_1(\infty)$  into determine the substantial appearance by the investigated problem.

### Finite element formulation

Whenever  $F'_1 = h$ ,  $h' = p$  and  $G'_1 = q$ , when entire component model by the residuals for binary nonlinear system based on boundary value problem (7)–(10), (16) and (17) over the typical element  $(\eta_e, \eta_{e+1})$  is

$$\int_{\eta_e}^{\eta_{e+1}} w_1 [F'_1 - h] d\eta = 0, \quad (27)$$

$$\int_{\eta_e}^{\eta_{e+1}} w_2 [h' - p] d\eta = 0, \quad (28)$$

$$\int_{\eta_e}^{\eta_{e+1}} w_3 [G'_1 - q] d\eta = 0, \quad (29)$$

$$\int_{\eta_e}^{\eta_{e+1}} w_4 [p' + G_1^2 + 2F_1 p - h^2 + K(2h p' + p^2 + q^2 - 2F_1 p'') + M(E_1 - h)] d\eta = 0, \quad (30)$$

$$\int_{\eta_e}^{\eta_{e+1}} w_5 [q' - 2h G_1 + 2F_1 q + K(-2F_1 q' + 2h q'') + M(E_1 - G_1)] d\eta = 0, \quad (31)$$

$$\int_{\eta_e}^{\eta_{e+1}} w_6 \left[ \begin{array}{l} \theta''_1 - 2\text{Pr} h \theta_1 + 2\text{Pr} F_1 \theta'_1 \\ + \text{Pr} Ec \{ (p^2 + q^2) \\ + M[(h - E_1)^2 + (G_1 - E_1)^2] \} \\ + \text{Pr} Ec K \{ h(p^2 + q^2) \\ - 2F_1 (pp' + qq') \} + Ah + B\theta_1 \end{array} \right] d\eta = 0, \quad (32)$$

where  $w_i (i=1, 2, 3, 4, 5, 6)$ , the weight action into reduces the fragment is approximate for  $F_1, h, p, G_1, q$  and  $\theta_1$  remain relative separately coming Galerkin finite development.

$$\left. \begin{array}{l} F_1 = \sum_{j=1}^2 F_j \Psi_j, h = \sum_{j=1}^2 h_j \Psi_j, p = \sum_{j=1}^2 p_j \Psi_j, G_1 = \sum_{j=1}^2 G_j \Psi_j, \\ q = \sum_{j=1}^2 q_j \Psi_j, \theta_1 = \sum_{j=1}^2 \theta_j \Psi_j, j = 1, 2 \end{array} \right\} \quad (33)$$

where  $F_j, h_j, p_j, G_j, q_j$  and  $\theta_j$  is the exotic nodal values and  $\Psi_j$  is linear shape functions which are detailed as

$$\Psi_j = (-1)^{j-1} \frac{\eta_{j+1} + \eta}{\eta_{j-1} + \eta_j}, j = 1, 2 \quad (34)$$

The system of equations is

$$\begin{bmatrix} K_{ij}^{11} & K_{ij}^{12} & K_{ij}^{13} & K_{ij}^{14} & K_{ij}^{15} & K_{ij}^{16} \\ K_{ij}^{21} & K_{ij}^{22} & K_{ij}^{23} & K_{ij}^{24} & K_{ij}^{25} & K_{ij}^{26} \\ K_{ij}^{31} & K_{ij}^{32} & K_{ij}^{33} & K_{ij}^{34} & K_{ij}^{35} & K_{ij}^{36} \\ K_{ij}^{41} & K_{ij}^{42} & K_{ij}^{43} & K_{ij}^{44} & K_{ij}^{45} & K_{ij}^{46} \\ K_{ij}^{51} & K_{ij}^{52} & K_{ij}^{53} & K_{ij}^{54} & K_{ij}^{55} & K_{ij}^{56} \\ K_{ij}^{61} & K_{ij}^{62} & K_{ij}^{63} & K_{ij}^{64} & K_{ij}^{65} & K_{ij}^{66} \end{bmatrix} \begin{bmatrix} F \\ h \\ p \\ G \\ q \\ \theta \end{bmatrix} = \begin{bmatrix} b^1 \\ b^2 \\ b^3 \\ b^4 \\ b^5 \\ b^6 \end{bmatrix}, \quad (35)$$

where

$$\begin{aligned}
K_{ij}^{11} &= \int_{\eta_e}^{\eta_{e+1}} \Psi_i \frac{d\Psi_j}{d\eta} d\eta, K_{ij}^{12} = - \int_{\eta_e}^{\eta_{e+1}} \Psi_i \Psi_j d\eta, \\
K_{ij}^{13} &= 0, K_{ij}^{14} = 0, K_{ij}^{15} = 0, K_{ij}^{16} = 0, b_i^1 = 0, \\
K_{ij}^{22} &= \int_{\eta_e}^{\eta_{e+1}} \Psi_i \frac{d\Psi_j}{d\eta} d\eta, K_{ij}^{23} = - \int_{\eta_e}^{\eta_{e+1}} \Psi_i \Psi_j d\eta, K_{ij}^{21} = 0, \\
K_{ij}^{24} &= 0, K_{ij}^{25} = 0, K_{ij}^{26} = 0, b_i^2 = 0, \\
K_{ij}^{34} &= \int_{\eta_e}^{\eta_{e+1}} \Psi_i \frac{d\Psi_j}{d\eta} d\eta, K_{ij}^{35} = - \int_{\eta_e}^{\eta_{e+1}} \Psi_i \Psi_j d\eta, K_{ij}^{31} = 0, \\
K_{ij}^{32} &= 0, K_{ij}^{33} = 0, K_{ij}^{36} = 0, b_i^3 = 0, \\
K_{ij}^{42} &= \int_{\eta_e}^{\eta_{e+1}} (-\bar{h}\Psi_i\Psi_j - M\Psi_i\Psi_j) d\eta, K_{ij}^{44} = \int_{\eta_e}^{\eta_{e+1}} (\bar{G}\Psi_i\Psi_j) d\eta, \\
K_{ij}^{45} &= \int_{\eta_e}^{\eta_{e+1}} (K\bar{q}\Psi_i\Psi_j) d\eta, \\
K_{ij}^{43} &= \int_{\eta_e}^{\eta_{e+1}} \left( \Psi_i \frac{d\Psi_j}{d\eta} + \bar{F}\Psi_i\Psi_j + K\bar{h}\Psi_i \frac{d\Psi_j}{d\eta} + K\bar{p}\Psi_i\Psi_j + K\bar{F} \frac{d\Psi_i}{d\eta} \frac{d\Psi_j}{d\eta} \right) d\eta, K_{ij}^{41} = 0, \\
K_{ij}^{46} &= 0, b_i^4 = 2K\bar{F}_1 \left( \Psi_i \frac{dp}{d\eta} \right)_{\eta_e} \\
&\quad - ME_1 \int_{\eta_e}^{\eta_{e+1}} \Psi_i d\eta, K_{ij}^{51} = 0, K_{ij}^{52} = \int_{\eta_e}^{\eta_{e+1}} (2\bar{G}\Psi_i\Psi_j) d\eta, K_{ij}^{53} = 0, K_{ij}^{56} = 0, \\
K_{ij}^{54} &= \int_{\eta_e}^{\eta_{e+1}} (-M\Psi_i\Psi_j) d\eta, K_{ij}^{43} = \int_{\eta_e}^{\eta_{e+1}} \left( \Psi_i \frac{d\Psi_j}{d\eta} + 2\bar{F}\Psi_i\Psi_j + 2\bar{F}K \frac{d\Psi_i}{d\eta} \frac{d\Psi_j}{d\eta} + 2K\bar{h}\Psi_i \frac{d\Psi_j}{d\eta} \right) d\eta, \\
b_i^5 &= 2K\bar{F}_1 \left( \Psi_i \frac{dq}{d\eta} \right)_{\eta_e} - ME_1 \int_{\eta_e}^{\eta_{e+1}} \Psi_i d\eta, K_{ij}^{61} = 0, K_{ij}^{62} = \int_{\eta_e}^{\eta_{e+1}} (\text{Pr}EcM\bar{h} - 2\text{Pr}EcME_1 + A)\Psi_i\Psi_j d\eta, \\
K_{ij}^{63} &= \int_{\eta_e}^{\eta_{e+1}} \left[ (\text{Pr}Ec\bar{p} + \text{Pr}EcK\bar{h}\bar{p})\Psi_i\Psi_j - 2\text{Pr}EcK\bar{F}\bar{p}\Psi_i \frac{d\Psi_j}{d\eta} \right] d\eta, \\
K_{ij}^{64} &= \int_{\eta_e}^{\eta_{e+1}} (\text{Pr}EcM\bar{h} - 2\text{Pr}EcME_1)\Psi_i\Psi_j d\eta, b_i^6 = - \left( \Psi_i \frac{d\theta_1}{d\eta} \right)_{\eta_e} - 2ME_1^2 \text{Pr}Ec \int_{\eta_e}^{\eta_{e+1}} \Psi_i d\eta, \\
K_{ij}^{65} &= \int_{\eta_e}^{\eta_{e+1}} \left[ (\text{Pr}Ec\bar{q} + \text{Pr}EcK\bar{h}\bar{q})\Psi_i\Psi_j - 2\text{Pr}EcK\bar{F}\bar{q}\Psi_i \frac{d\Psi_j}{d\eta} \right] d\eta, \\
K_{ij}^{66} &= \int_{\eta_e}^{\eta_{e+1}} \left[ (-2\text{Pr}\bar{h} + B)\Psi_i\Psi_j + 2\text{Pr}\bar{F}\Psi_i \frac{d\Psi_j}{d\eta} - \frac{d\Psi_i}{d\eta} \frac{d\Psi_j}{d\eta} \right] d\eta.
\end{aligned}$$

The nonlinear system about algebraic equations was transformed within linear system by algebraic equations along with applying Picard's linearization that recommends by the ensuing

$$\left. \begin{aligned} \bar{F} &= \sum_{j=1}^2 \bar{F}_j \Psi_j, \quad \bar{h} = \sum_{j=1}^2 \bar{h}_j \Psi_j, \quad \bar{p} = \sum_{j=1}^2 \bar{p}_j \Psi_j, \\ \bar{q} &= \sum_{j=1}^2 \bar{q}_j \Psi_j, \quad \bar{G} = \sum_{j=1}^2 \bar{G}_j \Psi_j, \quad j = 1, 2 \end{aligned} \right\} \quad (36)$$

where  $\bar{F}_i$ ,  $\bar{h}_i$ ,  $\bar{q}_i$ ,  $\bar{p}_i$ , and  $\bar{G}_i$  remain the exotic nodal values and computed by the earlier iteration.

## Validation of results

Graphical investigation during the applicable parameters was absolutely essential through justify our estimated result. In Table 1, we had related our explanation along with such based on Ariel<sup>36</sup> and Burhan Jafeer and Mustafa<sup>12</sup> for different values of  $M$  is the attached case being skin friction values and Table 2, we compared our solutions with Burhan Jafeer and Mustafa<sup>12</sup> for rate by heat transfer values as various values about  $K$  and  $Pr$ . In both tables, could be certain visual to ensuing performance by the suggested reaching was also precise and follow acceptable arrangement for every convenient impact to the article.

## Results and discussion

This section addresses the effect of the dynamic parameters of viscoelastic fluid through tables and graphs. Numeric productivity had heat transport and frictional factor was determined and abstracted through regression analysis. They studied as parametric values by  $K = 0.5$ ,  $M = 0.5$ ,  $Pr = 0.71$ ,  $Ec = 0.5$ ,  $S = 0.5$ ,  $E_1 = 0.01$ ,  $A = 0.1$  and  $B = 0.1$  unless otherwise stated.

Figures 2–4 displays the results of change of magnetic communication parameters with both electric field and electric field absence. Physically, electric field increase in Lorentz force when behaves by the accelerating force and reduces the fluid friction that causes to change of integration further the permeable disk. It is found that the velocity curve behaves opposite for electric and magnetic fields. Inferior magnetic field, boundary layer was considerably blended compared to the case of the not magnetic field. The pair of circular and radial flows show decreases when the existence by Lorentz force. Downtrend of appropriated flow caused by Lorentz force decreases the amount of cold fluid absorb into the disk. Temperature in Figure 4 exhibits the linear communication for  $M$ . Every viscous hindrance stemming when  $M$  produces friction among fluid surface and molecules, which translates frictional energy within thermal energy. Furthermore, from these graphs, this is supported to velocity other than the thickness of boundary layer decreased to enhancement on suction parameter ( $S > 0$ ). The role of suction was the being the fluid conclusion thus drops and surface the radial and circular velocities, whereas reverse direction was esteemed being injection parameter ( $S < 0$ ), by injection benefit the

flow of full extra into fluid stream. Temperature rises from injection and suction. Fair improvement is exhibited in Figure 4. From injection, thermal improvement was extra clear-cut in that as suction. Essentially, injection grants extra fluid for full central the place, time to consumption fluid leaves the locality. Hence, the existence of extra insignificant metallic particles at the time of injection aids the systems that consume extra temperature.

Figures 5 and 6 show the transformation to velocity components with viscoelastic fluid parameter  $K$  upto 2.0 for both hydrodynamic and hydromagnetic flow situations. Figure 5 shows the radial velocity proportional to  $F'_1$ , increase upon developing  $K$  for suction. This phenomenon is opposite for injection. That means this radially noticeable flow produces as disk outward development stimulates in raising values of  $K$ . Surrounding motion was fully decorated when the inclusion of elasticity effects. That result is away from surprise for elastic forces act by tensile stresses that influence for open up the fluid flow. Figures 5 and 6 clear up this the boundary layer thickness increases extremely as raising  $K$  values and break the continual value was  $K$  tend to infinity ( $K \rightarrow \infty$ ).

Importance to viscous dissipation of the flow figure, we measure temperature curves on different values of Eckert number  $Ec$  and of Prandtl number  $Pr$  and is exhibited in Figure 7. It is noticed that the gain to Prandtl number  $Pr$  causes devaluation to the temperature sketch. Even the reason for this downturn as the lesser values of Prandtl number  $Pr$  was equivalent to greater thermal conductivity. Therefore, the thermal conductivity is higher, the temperature was greater. A high Prandtl number coincides into small thermal conductivity and reduces temperature flow. Further, the greater values to the Eckert number  $Ec$ , the temperature distribution increases and the thermal boundary layer become delicate. Eckert number  $Ec$  was the ratio for the kinetic energy about fluid and enthalpy. Since expanding values of the kinetic energy increases, Eckert number  $Ec$  that causes an improvement of fluid temperature for both suction and injection. By the injection in Figure 7, they identify extra district summary of temperature by related that consumption being to injection extra fluid arrive surround the boundary layer region. Hence, the thermal achievement develops into extra clear-cut.

Variation the temperature sketch toward capacity and temperature-vulnerable heat generation/absorption parameters were investigated in Supplemental Figure 8 for both suction and injection. That predictable, the developing values by heat source ( $A > 0$ ) intensify of fluid temperature raised the disk, although as the case from  $A < 0$  energy was involved, subsequent to the temperature to fall. Further, this plot demonstrates of energy was forwarded during  $B$  rises, that appreciate the temperature, although energy was involved as overcast the values of  $B < 0$  causing important temperature drop near the boundary layer. Furthermore, the volume of appropriated fluid is approximated to rise on the continuation of digestion. When that reason, one predicts temperature sketch for growing expansive whenever  $S$  as incremented.

Nature of  $M$  and  $E_1$  with radial skin friction coefficient is plotted through Supplemental Figure 9 for suction case and

**Table 1.** Comparison of FEM results with those obtained by Ariel,<sup>36</sup> Burhan Jafeer and Mustafa<sup>12</sup> since various values as  $M$  at  $S = 0.0$ ,  $E = 0.0$ ,  $\beta = 0.0$ , and  $Ec = 0.0$ .

$M$	Ariel <sup>36</sup>		Burhan Jafeer and Mustafa <sup>12</sup>		Present results	
	$F_1''(0)$	$G_1'(0)$	$F_1''(0)$	$G_1'(0)$	$F_1''(0)$	$G_1'(0)$
0.2	0.453141	0.708795	0.453129	0.708793	0.4531409	0.7087953
0.4	0.405576	0.802376	0.405576	0.802376	0.4055757	0.8023764
0.6	0.366698	0.894476	0.366698	0.894476	0.3666980	0.8944758
0.8	0.335092	0.983607	0.335090	0.983607	0.3350897	0.9836071
1.0	0.309258	1.069053	0.309258	1.069053	0.3092580	1.0690534
1.2	0.287915	1.150635	0.287915	1.150635	0.2879154	1.1506349
1.4	0.270049	1.228466	0.270049	1.228466	0.2700490	1.2284662
1.6	0.254892	1.302793	0.254892	1.302793	0.2548924	1.3027934
2.0	0.230559	1.442094	0.230559	1.442094	0.2305591	1.4420940

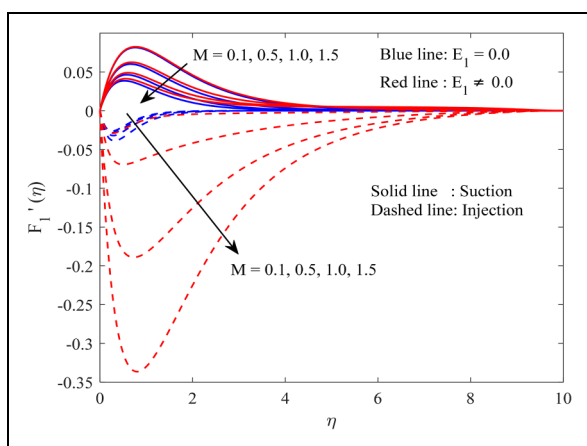


**Figure 2.** Velocity  $F_1'$  versus  $M$  for  $E_1 = 0.0$  and  $E_1 \neq 0.0$ .

Supplemental Figure 10 for injection. Consideration certified to accession in values of both magnetic and electric fields extended of radial skin friction at the rates 0.0317 and 0.689887 for suction, and 2.274723 and 2.701589 for injection. The essential cause was to magnetic field attack by flow of viscoelastic fluid completed disk surface when outstanding magnetic effects than intensity  $C_{ff}$ . Hence, the character of the disk surface would be extra drag concerned from injection.

Nature of skin friction coefficient against  $M$  and  $E_1$  is displayed in Supplemental Figure 11 for digestion and Supplemental Figure 12 from injection, respectively. It is observed that circular skin friction coefficient increases in case of electric force, whereas it decreases for the case of magnetic field. The continuous relapse slope acknowledge of accession in electric field was suction by the rate 0.309222, although it was decreased in magnetic field at the rate  $-0.33909$  in suction case. The circular drag force increases for both electric and magnetic fields in case of injection. Slope analysis determines the increment by the rate 1.009222 as electric field, while it was 0.662136 for magnetic field. This result shows higher circular skin friction from injection by correlated with suction. Therefore, the surface would be limited drag concerned about suction.

**Table 2.** Comparison of FEM results with those obtained by Burhan Jafeer and Mustafa<sup>12</sup> since various values of  $K$  and  $Pr$  at  $S = 0.5$ ,  $E = 0.0$ ,  $M = 0.5$ ,  $\beta = 0.0$ , and  $Ec = 0.5$ .

$K$	$Pr$	$-\theta_1'(0)$	
		Burhan Jafeer and Mustafa <sup>12</sup>	Present results
0	1.25	0.82472	0.826216
	0.4	0.77491	0.774819
	0.8	0.74014	0.742699
	1.5	0.73779	0.699987
0.5	0.5	0.24414	0.243847
	0.8	0.36261	0.362397
	1.25	0.52650	0.526497
	1.75	0.70029	0.699851

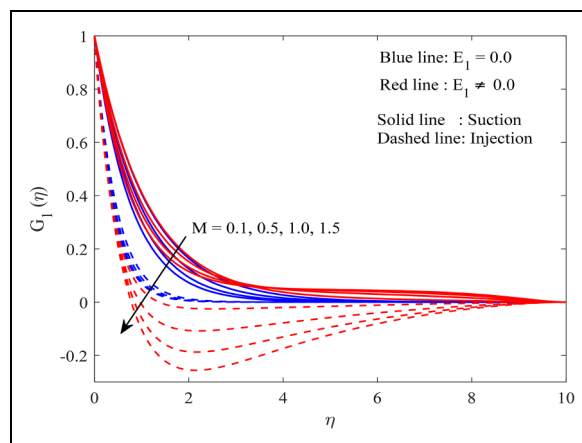


**Figure 3.** Velocity  $G_1$  versus  $M$  for  $E_1 = 0.0$  and  $E_1 \neq 0.0$ .

Impacts of  $M$  and  $E_1$  on heat transfer rate are disclosed in Supplemental Figure 13 for suction and Supplemental Figure 14 is shown for injection case. It was fair to the rate of heat transfer reduces as both magnetic and electric forces in suction, while it increased for injection. Heat transport in Supplemental Figure 13 decreased at the rate  $-1.28792$  for electric force and  $-0.14515$  for magnetic force. Electric field interprets the accession by the rate 0.199594 for injection, although magnetic field

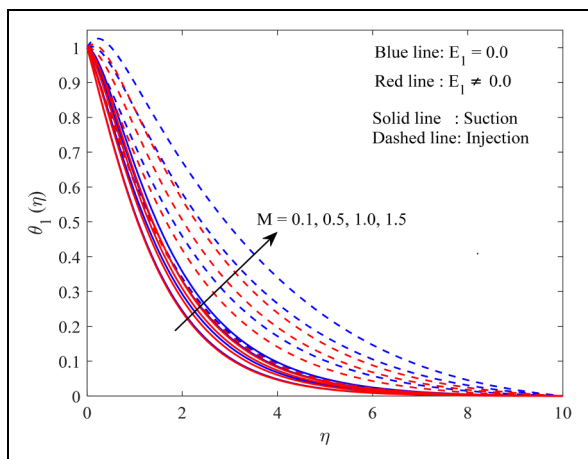


**Figure 4.** Temperature  $\theta_1$  versus  $M$  for  $E_1 = 0.0$  and  $E_1 \neq 0.0$ .

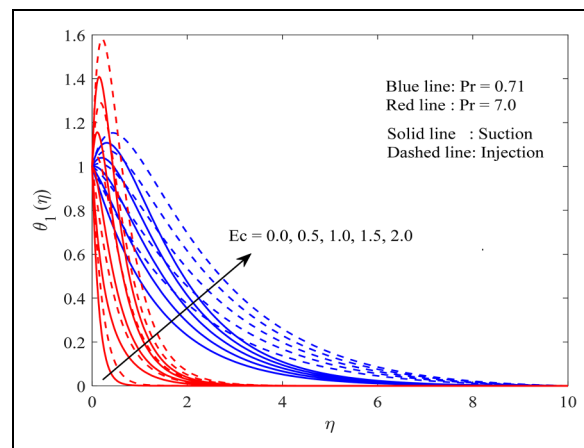


**Figure 7.** Temperature  $\theta_1$  versus  $Ec$  for  $Pr = 0.71$  and  $Pr \neq 7.0$ .

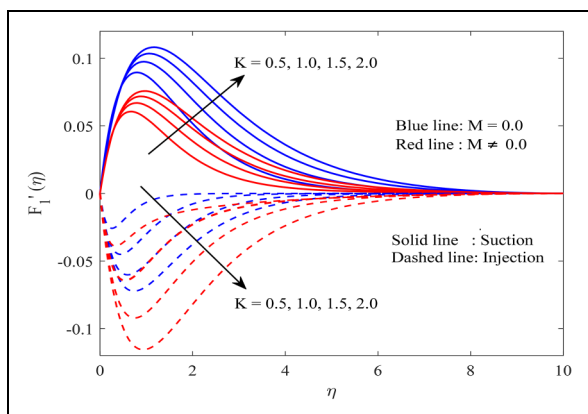


**Figure 5.** Velocity  $F_1'$  versus  $K$  about  $M = 0.0$  and  $M \neq 0.0$ .

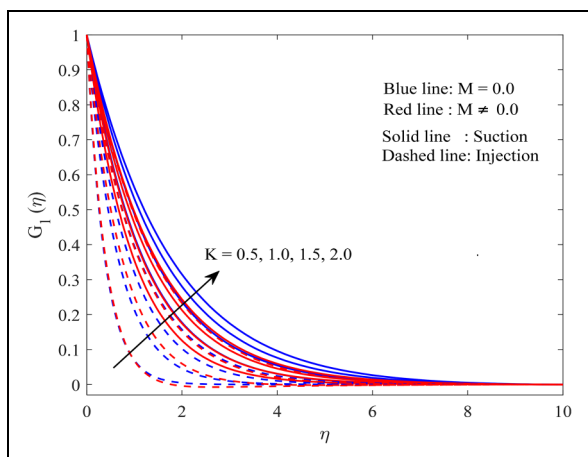


**Figure 6.** Velocity  $G_1$  versus  $K$  at  $M = 0.0$  and  $M \neq 0.0$ .

contributes 0.415269. Injection provides a higher heat transfer rate as compared to suction. Hence, the surface will be a greater heat transfer rate affected for injection.

Table 3 includes the computational impact on skin friction coefficients and Nusselt number. Every result predicts that radial drag force elevates, while circular drag

force decelerates due to the inclusion of elasticity effects. More, heat transfer rate resolved as Nusselt number decelerates as  $K$  turnout broad. Table 3 shows higher skin friction for injection related to digestion. The rate of accession of digestion is 0.419481 and it was 0.546785 from injection. The linear regression slope in Table 3 substantiates for heat transfer rate provides  $-0.02821$  for suction, while injection provides only  $-0.17884$ . Heat transport reduces on this table by the rate  $-0.74433$  from increasing  $Ec$  values being digestion, while it increases 0.680277 for injection for the case of air. For the case of  $Pr = 7.0$  (water), it will be  $-6.86083$  being digestion and 1.301476 from injection. Outside rate of heat transfer was considered for injection.

## Conclusions

This article investigates the heat transfer characteristics in von Kármán flow (of infinite disk) with second-grade fluid. The disk is assumed permeable with a prescribed (quadratic) temperature circulation  $T_w(r)$ . Electric and magnetic fields are included to have more realistic results. Additionally, space and temperature-dependent heat source/sink are also included. Governing equations through a similarity approach are solved using an innovative FEM. From this analysis, some of the key observations are as follows:

1. Viscoelastic fluid flow accelerated with elastic parameter yet decelerated from magnetic parameter. Suction shows high velocities by related to injection. Electric and magnetic fields have opposite behavior in velocity distributions.
2. Skin friction coefficients are raised with couple of electric and magnetic fields. Approximately more effect is contributed by injection.
3. Temperature is reduced with heat sink parameter and Prandtl number, while rest of the parameters explores the opposite effect. Injection exhibits increasing thermal outcome as compared to suction. Thus in

**Table 3.** The skin friction coefficients and Nusselt number values being various physical parameters.

Pr	K	Ec	Suction			Injection		
			$Re^{1/2}C_{fr}$	$\frac{2}{\pi} Re^{1/2}C_{m,r}$	Nu	$Re^{1/2}C_{fr}$	$\frac{2}{\pi} Re^{1/2}C_{m,r}$	Nu
0.71	0.1	0.5	0.40768393	-1.14786155	0.36292882	0.42921114	3.11184700	0.49524948
			0.66796206	-1.21282689	0.34835838	0.79869882	2.94866551	0.29767795
	1.0	0.89356820	-1.26414188	0.33408360	1.08493290	2.81994709	0.20840297	
	1.5	1.07033565	-1.30104949	0.32101475	1.30751956	2.72162533	0.15951412	
	2.0	1.21906382	-1.33007419	0.30870889	1.49619043	2.64367660	0.12780575	
	Slope		<b>0.419481</b>	<b>-0.09358</b>	<b>-0.02821</b>	<b>0.546785</b>	<b>-0.24065</b>	<b>-0.17884</b>
	0.5	0.0			0.72052246			-0.04246041
		0.5			0.34835838			0.29767795
		1.0			-0.02380570			0.63781631
		1.5			-0.39596978			0.97795467
7.0	0.1	0.5			-0.76813385			1.31809303
					<b>-0.74433</b>			<b>0.680277</b>
	0.5		3.96360962					1.70384806
	1.0		3.63878107					0.64547597
	1.5		3.36980592					0.40350087
	2.0		3.16565339					0.30004944
	Slope		<b>-0.49779</b>					<b>-0.66338</b>
	0.5	0.0			7.06919855			-0.00526195
		0.5			3.63878107			0.64547597
		1.0			0.20836362			1.29621389
	1.5			-3.22205383			1.94695181	
	2.0			-6.65247128			2.59768973	
	Slope			<b>-6.86083</b>			<b>1.301476</b>	

this situation, suction becomes effective for cooling procedure.

- Suction contributes to the reduction in temperature, but the injection produces the growth for the same.
- Eckert number and viscoelastic fluid parameter provide the reduction in heat transfer, whereas Prandtl numbers provide the enhancement. Injection provides a higher heat transfer rate.
- The rate of heat transfer decreases by 36.41% for suction and 49.67% for injection with variation in viscoelastic parameter.

Based on the present analysis, it can be assumed proposed method can serve as an inspiration for further models of viscoelastic fluid flow. As a variation in temperature causes fluctuations in a flow configuration with temperature-dependent heat source and suction or injection is more accurate and reliable. Hence, this research can be used in various environmental and engineering processes such as heat transfer (cooling and heating), biomedicine, energy savers, and nuclear reactors. In further, the study can be extended to viscoelastic nanoparticles.

### Acknowledgments

The authors are very grateful to the editor and reviewers for their constructive suggestions.



### Declaration of conflicting interests

The author(s) declared no potential conflicts of interest with respect to the research, authorship, and/or publication of this article.

### Funding

The author(s) received no financial support for the research, authorship, and/or publication of this article.

### ORCID iDs

Kotha Gangadhar  <https://orcid.org/0000-0002-0264-2512>  
M. Rupa Lavanya  <https://orcid.org/0000-0002-8040-0607>

### Supplemental material

Supplemental material for this article is available online.

### References

- Daniel YS, Aziz ZA, Ismail Z, et al. Slip role for unsteady MHD mixed convection of nanofluid over stretching sheet with thermal radiation and electric field. *Indian J Phys* 2020; 94: 195–207.
- Mardani MR, Ganji DD and Hosseinzadeh Kh. Numerical investigation of droplet coalescence of saltwater in the crude oil by external electric field. *J Mol Liq* 2022; 346: 117111.
- Sun Y, Kang Z, Ma S, et al. Heat transfer model for electrochromatography in transverse electric field. *Int J Therm Sci* 2022; 172: 107336.
- Khazayinejad M and Nourazar SS. On the effect of spatial fractional heat conduction in MHD boundary layer flow using gr-Fe<sub>3</sub>O<sub>4</sub>-H<sub>2</sub>O hybrid nanofluid. *Int J Therm Sci* 2022; 172: 107265.
- Urgorri FR, Moreno C, Fernandez-Berceruelo I, et al. The influence of MHD boundary layers on tritium permeation

- in PbLi flows for fusion breeding blankets. *Int J Heat Mass Transf* 2021; 181: 121906.
6. Zhang L, Li X, Liu X, et al. The influence of second-harmonic generation under the external electric field and magnetic field of parabolic quantum dots. *Physica B: Condens Matter* 2021; 618: 413197.
  7. Yan XF, Tian MY, Yan J, et al. In-plane electric and exchange fields engineered corner state bismuthene quantum dots. *Physica B: Condens Matter* 2022; 630: 413641.
  8. Zakaria K, Kamel H and Gamiel Y. Instability of a viscous liquid sheet under the influence of a tangential electric field. *Alex Eng J* 2022; 61: 5169–5181.
  9. Siddiqui BK, Batool S, Hassan QM, et al. Irreversibility analysis in the boundary layer MHD two dimensional flow of Maxwell nanofluid over a melting surface. *Ain Shams Eng J* 2021; 12: 3217–3227.
  10. Riaz Khan M, Mao S, Deebani W, et al. Numerical analysis of heat transfer and friction drag relating to the effect of Joule heating, viscous dissipation and heat generation/absorption in aligned MHD slip flow of a nanofluid. *Int Commun Heat Mass Transf* 2022; 131: 105843.
  11. Korei Z, Benissaad S, Berrahil F, et al. MHD Mixed convection and irreversibility analysis of hybrid nanofluids in a partially heated lid-driven cavity chamfered from the bottom side. *Int Commun Heat Mass Transf* 2022; 132: 105895.
  12. Burhan Jafeer M and Mustafa M. A novel formulation and analysis for heat transfer in von kármán flow involving viscoelastic fluid: OHAM solutions. *J Therm Anal Calorim* 2022; 147: 477–488.
  13. Hafeez A, Khan M and Ahmed J. Flow of magnetized oldroyd-B nanofluid over a rotating disk. *Appl Nanosci* 2020; 10: 5135–5147.
  14. Gupta S, Chauhan A and Sasmal C. Influence of elastic instability and elastic turbulence on mixed convection of viscoelastic fluids in a lid-driven cavity. *Int J Heat Mass Transf* 2022; 186: 122469.
  15. Hernández A, Arcos J, Martínez-Trinidad J, et al. Thermodiffusive effect on the local Debye-length in an electroosmotic flow of a viscoelastic fluid in a slit micro-channel. *Int J Heat Mass Transf* 2022; 187: 122522.
  16. Cao C and Kraume M. Axial thrust and power consumption of propellers in viscoelastic fluids exhibiting hysteresis effect. *Chem Eng Sci* 2022; 248: 117237.
  17. Venkata Ramana K, Gangadhar K, Kannan T, et al. Cattaneo-Christov heat flux theory on transverse MHD oldroyd-B liquid over nonlinear stretched flow. *J Therm Anal Calorim* 2022; 147: 2749–2759.
  18. Salahuddin T, Siddique N, Khan M, et al. A significant study on flow analysis of viscoelastic fluid with variable thermo-physical properties. *Math Comput Simul* 2022; 194: 416–429.
  19. Meng Y and Li B. On viscoelastic fluid in a vertical porous media channel with sores and dufour effects. *Appl Math Lett* 2022; 124: 107656.
  20. Khan M, Iqbal Z and Ahmed A. A mathematical model to examine the heat transport features in burgers fluid flow due to stretching cylinder. *J Therm Anal Calorim* 2022; 147: 827–841.
  21. Liu S, Yang W and Zheng L. Modeling and analysis of double fractional order Jeffreys viscoelastic fluids flow. *Appl Math Lett* 2022; 124: 107630.
  22. Oke AS. Theoretical analysis of modified eyring powell fluid flow. *J Taiwan Inst Chem Eng* 2022; 132: 104152.
  23. Pimenta F and Alves MA. Conjugate heat transfer in the unbounded flow of a viscoelastic fluid past a sphere. *Int J Heat Fluid Flow* 2021; 89: 108784.
  24. Chen X, Jian Y and Xie Z. Slippery electrokinetic flow of viscoelastic fluids with pressure-dependent viscosity and relaxation time. *Colloids Surf A Physicochem Eng Asp* 2022; 639: 128354.
  25. Akhtar S, Jamil S, Shah NA, et al. Effect of zeta potential on fractional pulsatile electroosmotic flow of Maxwell fluid. *Chin J Phys* 2022; 76: 59–67.
  26. Nazir U, Saleem S, Nawaz M, et al. Three-dimensional heat transfer in nonlinear flow: a FEM computational approach. *J Therm Anal Calorim* 2020; 140: 2519–2528.
  27. Singh AK, Kuamr A and Singh AK. Effect of non-uniform heating and viscous dissipation on natural convective flow of Casson fluid over a vertical cone. *Indian J Phys* 2022; 96: 481–489.
  28. Mburu ZM, Nayak MK, Mondal S, et al. Impact of irreversibility ratio and entropy generation on three-dimensional oldroyd-B fluid flow with relaxation-retardation viscous dissipation. *Indian J Phys* 2022; 96: 151–167.
  29. Gangadhar K, EdukondalaNayak R, VenkataSubbaRao M, et al. Nodal/saddle stagnation point slip flow of an aqueous conventional magnesium oxide-gold hybrid nanofluid with viscous dissipation. *Arab J Sci Eng* 2021; 46: 2701–2710.
  30. Rao AS, Ramaiah KD, Kotha G, et al. A spectral relaxation approach for boundary layer flow of nanofluid past an exponentially stretching surface with variable suction in the presence of heat source/sink with viscous dissipation. *Arab J Sci Eng* 2021; 46: 7509–7520.
  31. Gangadhar K, Seshakumari PM, VenkataSubbaRao M, et al. MHD flow analysis of a Williamson nanfluid due to thomson and troian slip condition. *Int J Appl Comput Math* 2022; 8:6.
  32. Hamid RA, Nazar R, Naganthran K, et al. Dusty ferrofluid transport phenomena towards a non-isothermal moving surface with viscous dissipation. *Chin J Phys* 2022; 75: 139–151.
  33. Ajibade AO and Umar AM. Effect of wall conduction on steady natural convection outflow in a vertical channel. *Meccanica* 2021; 56: 2257–2267.
  34. Abbasi A, Khan SU, Farooq W, et al. Optimized analysis and enhanced thermal efficiency of copper-aluminum oxide nanoparticles under the influence of Joule heating and viscous dissipation. *Eur Phys J Plus* 2021; 136: 1026.
  35. Salawu SO, Kareem RA, Shamshuddin MD, et al. Double exothermic reaction of viscous dissipative oldroyd-80 constant fluid and thermal ignition in a channel. *Chem Phys Lett* 2020; 760: 138011.
  36. Ariel PD. On computation of MHD flow near a rotating disk. *J Appl Math Mech* 2002; 82: 235–246.
  37. Attia HA. The effect of ion slip on the flow of reiner-rivlin fluid due a rotating disk with heat transfer. *J Mech Sci Tech* 2007; 21: 174–183.
  38. Guha A and Sengupta S. Analysis of von Kármán swirling flow on a rotating disc in Bingham fluids. *Phys Fluids* 2016; 28: 013601.
  39. Kumar A, RK Ray and Sheremet MA. Entropy generation on double-diffusive slip flow of nanofluid over a rotating disk with nonlinear mixed convection and Arrhenius activation energy. *Indian J Phys* 2022; 96: 525–541.

40. Khan M, Salahuddin T and Stephen SO. Variable thermal conductivity and diffusivity of liquids and gases near a rotating disk with temperature dependent viscosity. *J Mol Liq* 2021; 333: 115749.
41. Mabood F, Rauf A, Prasannakumara BC, et al. Impacts of stefan blowing and mass convention on flow of Maxwell nanofluid of variable thermal conductivity about a rotating disk. *Chin J Phys* 2021; 71: 260–272.
42. Liu P, Cui X, Wang G, et al. An accurate and efficient scheme for linear and nonlinear analyses based on a gradient-weighted technique. *Int J Non Linear Mech* 2018; 105: 9–19.